Physica A 433 (2015) 356–366

Contents lists available at ScienceDirect

Physica A

journal homepage: www.elsevier.com/locate/physa

Noise-sustained synchronization between electrically coupled FitzHugh–Nagumo networks

Guadalupe Cascallares [a], Alejandro D. Sánchez [b,1], Matías G. dell'Erba [b,1], Gonzalo G. Izús [b,*,1]

[a] Centro Atómico Bariloche, San Carlos de Bariloche, R8402AGP Río Negro, Argentina

[b] IFIMAR (Universidad Nacional de Mar del Plata and CONICET), Deán Funes 3350, B7602AYL Mar del Plata, Argentina

HIGHLIGHTS

- Noise-sustained sync in two coupled rings of FitzHugh–Nagumo cells is investigated.
- Routes to sync are explained by the system's non equilibrium potential landscape.
- Noise for optimal sync is theoretically obtained and numerically confirmed.

ARTICLE INFO

Article history:
Received 10 November 2014
Received in revised form 9 March 2015
Available online 23 March 2015

Keywords:
Synchronization
FitzHugh-Nagumo
Electrical synapses
Non-equilibrium potential
Noise
Excitability

ABSTRACT

We investigate the capability of electrical synapses to transmit the noise-sustained network activity from one network to another. The particular setup we consider is two identical rings with excitable FitzHugh–Nagumo cell dynamics and nearest-neighbor antiphase intra-ring coupling, electrically coupled between corresponding nodes. The whole system is submitted to independent local additive Gaussian white noises with common intensity η, but only one ring is externally forced by a global adiabatic subthreshold harmonic signal. We then seek conditions for a particular noise level to promote synchronized stable firing patterns. By running numerical integrations with increasing η, we observe the excitation activity to become spatiotemporally self-organized, until η is so strong that spoils sync between networks for a given value of the electric coupling strength. By means of a four-cell model and calculating the stationary probability distribution, we obtain a (signal-dependent) non-equilibrium potential landscape which explains qualitatively the observed regimes, and whose barrier heights give a good estimate of the optimal noise intensity for the sync between networks.

1. Introduction

As it is well known, the core component of the brain is the neuron: an electrically excitable cell that processes and transmits information by electro-chemical signaling. Functionally related neurons connect to each other, to form neural networks allowing the functional integration of spatially segregated information in the nervous system [1,2]. Among the activities that neural networks perform as a whole, the process of neural synchronization is crucial, because it is involved in a variety of cognitive functions such as perceptual grouping, attention-dependent stimulus selection, routing of signals across

* Corresponding author.
E-mail addresses: sanchez@mdp.edu.ar (A.D. Sánchez), mdellerba@ifimar-conicet.gob.ar (M.G. dell'Erba), izus@mdp.edu.ar (G.G. Izús).

[1] Member of CONICET, Argentina.

http://dx.doi.org/10.1016/j.physa.2015.03.016
0378-4371/

distributed cortical networks, sensory-motor integration, working memory, and perceptual awareness [3]. In this process, brain regions fulfilling specific functions communicate for the purpose of establishing transient networks that accomplish perception, cognition, and action. In turn, it has been demonstrated in neuron models that neural synchronization is facilitated by the addition of optimal amounts of noise [4–7]. It is also important to emphasize that the synchronization process is relevant whatever the number of neurons involved, from minimal neural networks (neural pair) [8] to large ensembles of neurons as a whole (such as the cortex) [9]. Thus, it is not surprising that the phenomenon of synchronization is a major research focus in modern neuroscience [10–15].

There exist two ways in which neurons communicate, these are chemical and electrical synapses. While chemical synapses constitute the main mode of signal transmission between neurons, electrical synapses promote synchronous behavior in neural networks [16–18]. In fact, gap junctions allow for direct electric communication between cells [8]. They are typically formed from the juxtaposition of two hemi-channels (connection proteins), and allow the free movement of ions or molecules across the intercellular space separating the plasma membrane of one cell from that of another. Gap junction coupling is known to occur between many cell types, including pancreatic cells [19], heart cells [20], and astrocytes [21] to cite some examples. A remarkable characteristic of electrical synapses is its bidirectionality, which reflects the fact that the information is transmitted directly by current from one cell to the other.

In previous studies [22–25] we have been investigating the noise-sustained synchronization of regular networks of autonomous units with excitable FitzHugh–Nagumo (FHN) dynamics, coupled in electrical or phase-repulsive way. We have shown that synchronization involves the formation of antiphase states (APS)—nonequilibrium structures in which the neurons on the ring alternate regularly (except for noise-induced defects) their excitation states in space. In particular, we have made theoretical estimations of noise thresholds for activation and synchronization of the APS. This analysis was facilitated by the knowledge for these systems [26,27] of the nonequilibrium potential (NEP) [28]. The NEP is the non-equilibrium analog of a free energy, and provides deep insight on the dynamical mechanisms leading to pattern formation and other phenomena where fluctuations play a constructive role [29–31].

We focus now on the capability of the electrical synapses to transmit the noise-sustained network activity from one network to another. With this aim, we consider a model consisting of two identical networks – connected by electrical coupling between corresponding nodes – and find conditions under which a particular level of noise promotes synchronized stable firing patterns when only one network is externally forced by a subthreshold harmonic adiabatic signal. In particular, we prove that the synchronized stochastic-resonant dynamics of both networks can be explained in terms of eventual noise-sustained transitions between attractors, being the adiabatic change in the relative stability of attractors – ruled by the NEP – the fundamental ingredient that determines the dynamics and the relevant noise scales.

The paper is organized as follows. In Section 2 we briefly review the dynamic equations of the model; in Section 3 we provide numerical evidence of noise-sustained synchronization between networks, and characterize the constructive role of noise in the process. Then we elucidate the observed dynamics in terms of the NEP of a reduced description in Section 4, and collect our conclusions in Section 5.

2. The model

The FHN model is surely one of the most paradigmatic mathematical models in theoretical research on neural networks. It emerges as a two-dimensional simplification of the four-dimensional Hodgkin–Huxley one, in which only the membrane potential and a recovery variable are represented. In turn, the FHN model is an archetypal model of activator–inhibitor systems and the simplest representation of excitable firing dynamics; it is capable of displaying periodic oscillations, stable fixed points, and excitability [32]. The constructive effects of noise on the FHN model have been widely reported in literature in a variety of phenomena [29,33,34]. Examples include coherence resonance [35], stochastic resonance [31,36–39], and noise-sustained synchronization [40,41].

To analyze the synchronizability between networks of noise-sustained activity, we consider a minimal block of a structured FHN neuronal network, composed of two identical phase-repulsive coupled rings, one of them (network I) externally forced by a subthreshold periodic signal while the other (network II) is only electrically coupled with the first ring. Inside each network we suppose a first-neighbor antiphase-coupling among activator variables, which exhibits the capability to sustain noise-induced activity by a well established mechanism [23]. For the coupling between arrays we consider a situation wherein the coupling is proportional to the difference of presynaptic and postsynaptic membrane potentials. This electrical coupling corresponds to so-called gap-junctions. Coupling parameters are assumed to be independent of the presynaptic and postsynaptic membrane potentials, and can therefore be modeled by constants D and E. The equations for the model are

$$\dot{u}_i = bu_i(1-u_i^2) - v_i + S(t) - D(u_{i+1}+u_{i-1}) + E(p_i-u_i) + r_1\,\xi_i^{(u)}(t) + r_2\,\xi_i^{(v)}(t) \tag{1}$$

$$\dot{v}_i = \epsilon(\beta u_i - v_i + C) + r_3\,\xi_i^{(u)}(t) + r_4\,\xi_i^{(v)}(t) \tag{2}$$

$$\dot{p}_i = bp_i(1-p_i^2) - q_i - D(p_{i+1}+p_{i-1}) + E(u_i-p_i) + r_1\,\xi_i^{(p)}(t) + r_2\,\xi_i^{(q)}(t) \tag{3}$$

$$\dot{q}_i = \epsilon(\beta p_i - q_i + C) + r_3\,\xi_i^{(p)}(t) + r_4\,\xi_i^{(q)}(t). \tag{4}$$

The activator (u_i in network I, p_i in network II) is the fast variable, which mimics the action potential off cell i; the inhibitor (v_i in network I, q_i in network II) is the slow – or recovery – variable, which is related to the time dependent conductance

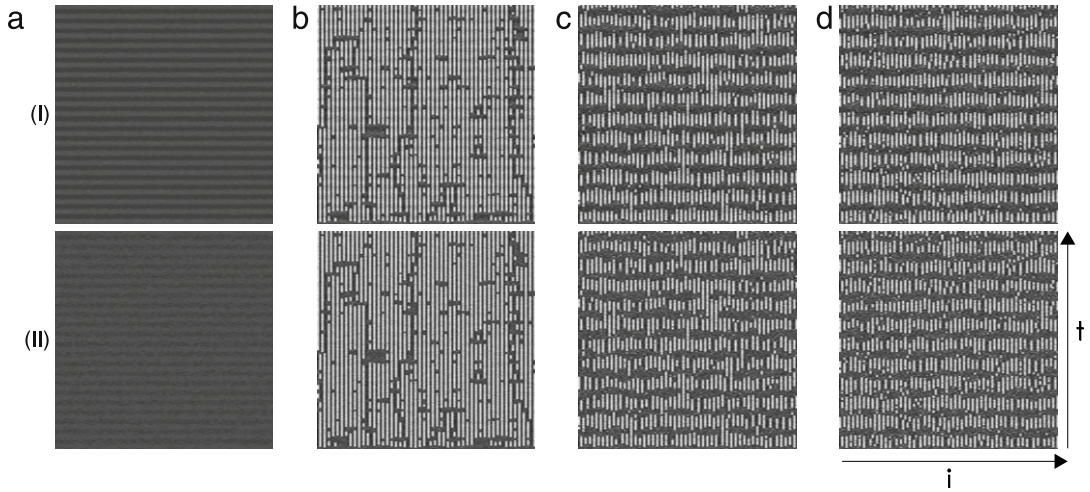

Fig. 1. Activity record of a subset of 100 neurons (until $t = 1.5 \times 10^5$) of network I (up) and II (down), for $E = 2 \times 10^{-2}$ and noise intensities: (a) 10^{-8}, (b) 3.5×10^{-7}, (c) 7×10^{-7}, and (d) 8.7×10^{-7}.

of the potassium channels in the membrane [42]. Here $i = 1, \ldots, N$; $u_{N+1} \equiv u_1$, $u_0 \equiv u_N$, $p_{N+1} \equiv p_1$, $p_0 \equiv p_N$. The subthreshold external signal $S = A_0 \sin \omega t$ is injected on all the nodes of network I only. ϵ is the activator–inhibitor timescales ratio, $D > 0$ is the antiphase-coupling strength within each network, while $E > 0$ is the electric coupling strength between networks. Finally, $\xi_i^{(k)}$ are Gaussian white noises with $\langle \xi_i^{(k)}(t) \rangle = 0$ and $\langle \xi_i^{(k)}(t)\, \xi_j^{(m)}(t') \rangle = \eta\ \delta_{i,j}\, \delta_{k,m}\, \delta(t - t')$, where η is the common noise intensity and $k, m \in \{u, v, p, q\}$.

Throughout the work, the following values have been adopted: $N = 256$, $\epsilon = \beta = 10^{-2}$, $b = 3.5 \times 10^{-2}$, $C = 2 \times 10^{-2}$, $D = 10^{-2}$, $A_0 = 1.1 \times 10^{-2}$, $\omega = 2 \times 10^{-3}$, $\epsilon\, r_1 = r_3 = \cos 0.05$ and $\epsilon\, r_2 = r_4 = \sin 0.05$. The values of the parameters are not totally arbitrary: the value of D is selected in order to have a well-developed regime of noise-sustained synchronization in an externally forced isolated network [24], while the period $T = 2\pi/\omega$ remains above the typical deterministic time (i.e. the turnaround time of a single spike), so that the signal can be regarded as an adiabatic perturbation. Besides, single-cell parameters have been selected in such a way that they satisfy an integrability condition, required by the theoretical characterization of the dynamics (see Eq. (11) in Section 4).

3. Noise sustained synchronization

We call activated or excited those cells for which the activator field exceeds some threshold value u_{th}. To quantify the level of activity of each network, we introduce the normalized global activity

$$A(t) = \frac{1}{N} \sum_{i=1}^{N} \Theta[x_i(t) - u_{th}]. \tag{5}$$

Here x_i represents either u_i or p_i (depending on the network we refer to), and Θ is the Heaviside step function. As expected, $A(t)$ is not sensitive to u_{th} for reasonable values of threshold. Hereafter we fix $u_{th} = 0.4$. Due to the fact that an excited neuron inhibits its network's neighbors through the antiphase-coupling, we often observe spatially alternating states of excited and inhibited cells, i.e. APS. Note that a perfect APS would correspond to $A = 1/2$. However, A does not reach, in general, this value because alternance fails due to the local noises.

To have a global view of the dynamics, in Fig. 1 we present the activity record of an equivalent subset of neurons of each ring, for $E = 2 \times 10^{-2}$ and different noise intensities. Numerical simulations of Eqs. (1)–(4) show that for small noise intensities, there are only small-amplitude homogeneous subthreshold oscillations around the rest state in each ring, as we show in Fig. 1(a). These coherent oscillations are induced by the adiabatic signal, and correspond to the homogeneous rest state.

As noise intensity increases, so does the number of cells that becomes active, and the networks are simultaneously driven to the APS (as shown in Fig. 1(b)). For higher levels of noise, the activity in both networks becomes simultaneously synchronized with the external signal, as shown in Fig. 1(c) and (d). Note that the APS is reached only when the signal is positive; when it is negative, all neurons remain in the rest state. A typical time series in the synchronized state can be seen in Fig. 2.

An indicator of the synchrony of each network with the external signal $S(t)$ is the Q-factor, defined by

$$Q = \sqrt{Q_{\sin}^2 + Q_{\cos}^2}, \quad \text{with} \tag{6}$$

$$Q_{\sin} = \frac{1}{nT} \int_0^{nT} 2A(t) \sin(\omega t) \mathrm{d}t$$

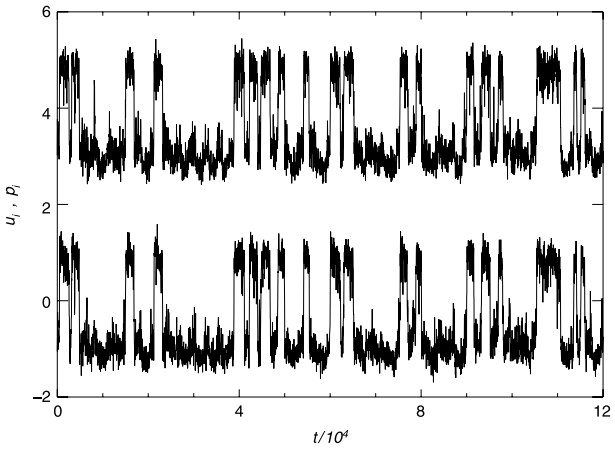

Fig. 2. Time evolution of activator fields of two electrically coupled neurons u_i (network I) and p_i (network II). Parameters are the same as in Fig. 1(c). The field p_i was shifted up four units for clarity.

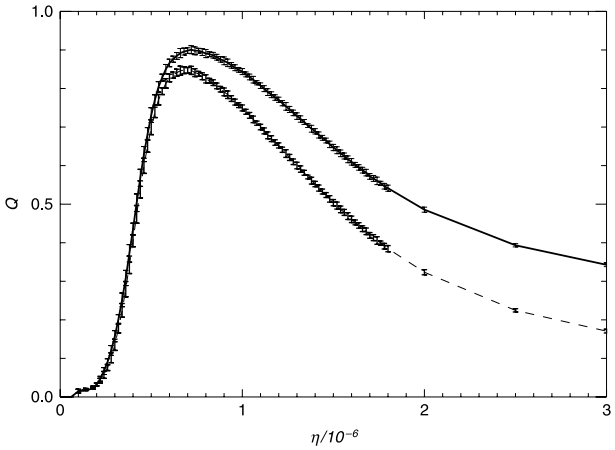

Fig. 3. Q-factor for network I (solid line) and network II (dashed line) as a function of noise intensity, averaged over 20 realizations and 44 signal periods, for $E = 2 \times 10^{-2}$.

$$Q_{\cos} = \frac{1}{nT} \int_0^{nT} 2A(t) \cos(\omega t) \mathrm{d}t,$$

where n is the number of periods T covered by the integration time. In Fig. 3 we show the Q-factor of each network as a function of noise intensity. Note that both curves reach a maximum for approximately the same noise intensity $\eta \approx 7 \times 10^{-7}$. The same scenario is observed for larger values of E.

Another useful estimator, in this case for the synchronization between networks' activities, is the correlation between the fields $\{u_i\}$ and $\{p_i\}$, given by

$$C(\{u_i\}, \{p_i\}, t) = \frac{\langle (u - \langle u \rangle)(p - \langle p \rangle) \rangle}{\sqrt{\langle (u - \langle u \rangle)^2 \rangle} \sqrt{\langle (p - \langle p \rangle)^2 \rangle}}, \tag{7}$$

where the brackets mean average over $\{u_i\}$ and $\{p_i\}$. In Fig. 4 we show the time evolution of the correlation for a typical realization of the system's equations. The high degree of synchronization between the network activities is apparent.

It is clear that the coupling term and the local noise drive the dynamics of network II. In particular, electrical synapses provide a fluctuating term with the same period of the external forcing. This point is illustrated in Fig. 5, where the averaged coupling term for network II is plotted vs. time for a typical realization of Eqs. (1)–(4).

Other dynamical regimes where only partial activation takes place are numerically observed for small electrical coupling values. Again, a minimum level of noise is required to drive the dynamics. We illustrate this point in Fig. 6, where the activity record of a subset of neurons of each network is shown for $E = 2 \times 10^{-3}$ and selected values of noise. While only small subthreshold oscillations develop in both rings for small η (panels a and b), network I can reach a synchronized regime for appropriate values of noise (panels c and d). In this process, network II remains at rest and no activity develops there.

Activating network II requires larger levels of noise. We illustrate this point in Fig. 7, where we show (for the same coupling intensity E) an APS in network II, while network I remains synchronized (panels a and b). Note that the APS is

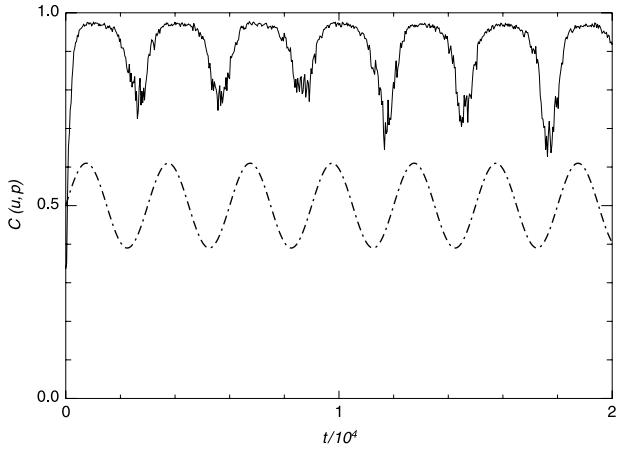

Fig. 4. Correlation (solid line) as a function of time, in a synchronized state, averaged over all the activator fields in both networks. The parameters are the same as in Fig. 1(c). As reference we include the signal (amplified by a factor 10 and shifted by 0.5 for clarity).

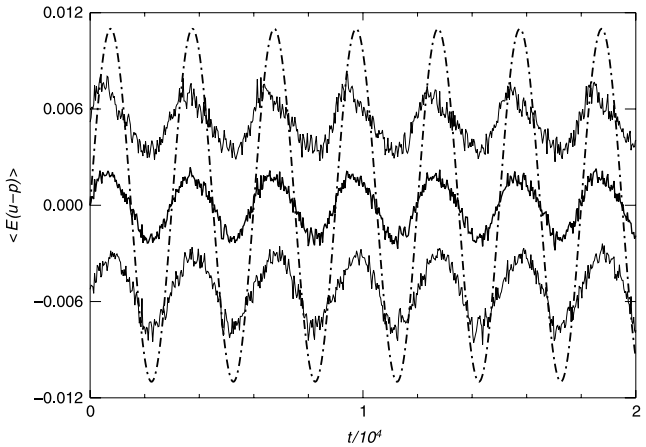

Fig. 5. Averaged coupling terms of network II (bold solid line). The signal (dashed-dotted line) was included as a reference. The additional solid lines correspond to the coupling term plus and minus its standard deviation. Parameters are the same as those of Fig. 1(c).

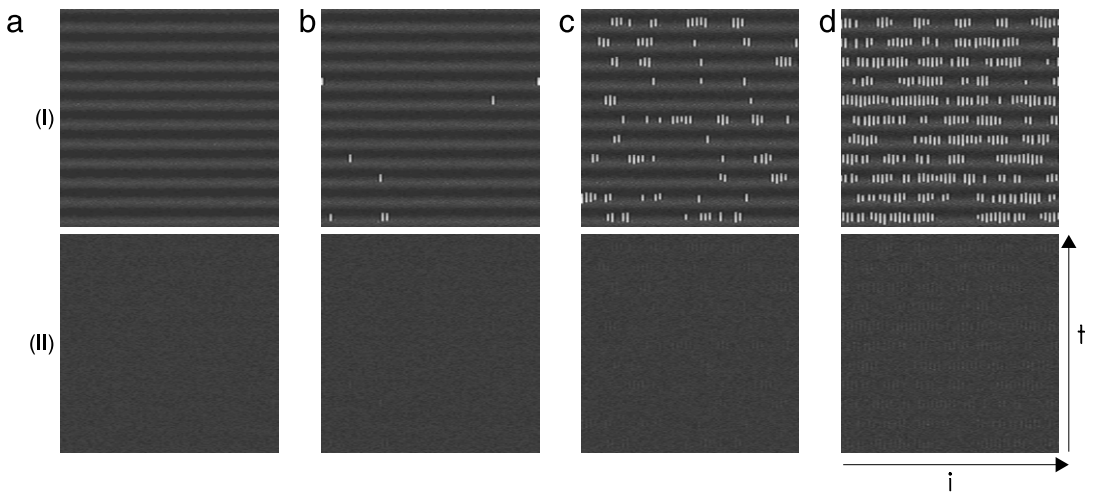

Fig. 6. Activity record of a subset of 100 neurons ($t = 3.3 \times 10^4$) of network I (up) and II (down), for $E = 2 \times 10^{-3}$ and noise intensities: (a) 2×10^{-8}, (b) 3×10^{-8}, (c) 4.7×10^{-8}, and (d) 7.7×10^{-8}.

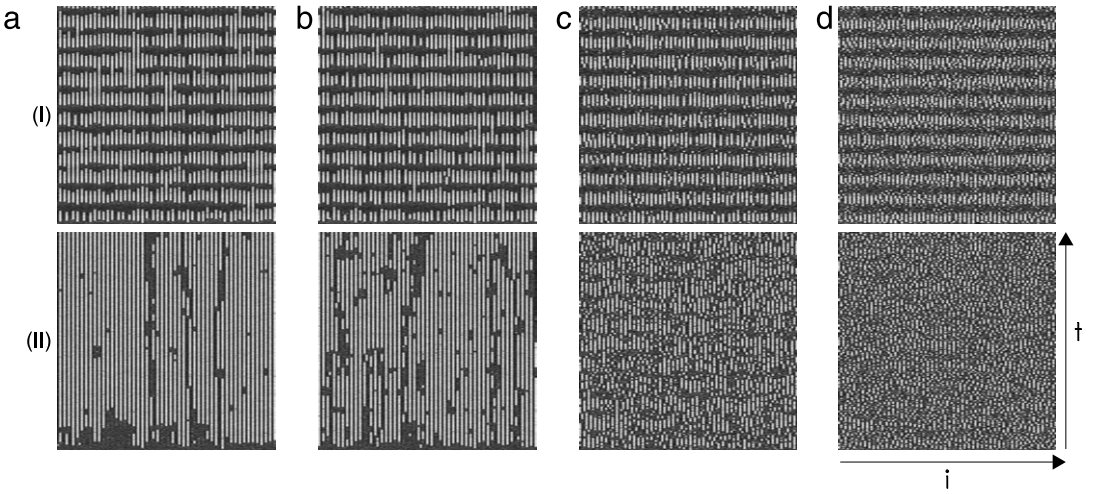

Fig. 7. Activity record of a subset of 100 neurons ($t = 3.3 \times 10^4$) of network I (up) and II (down), for $E = 2 \times 10^{-3}$ and noise intensities: (a) 2.5×10^{-7}, (b) 2.9×10^{-7}, (c) 4.5×10^{-7}, and (d) 7.3×10^{-7}.

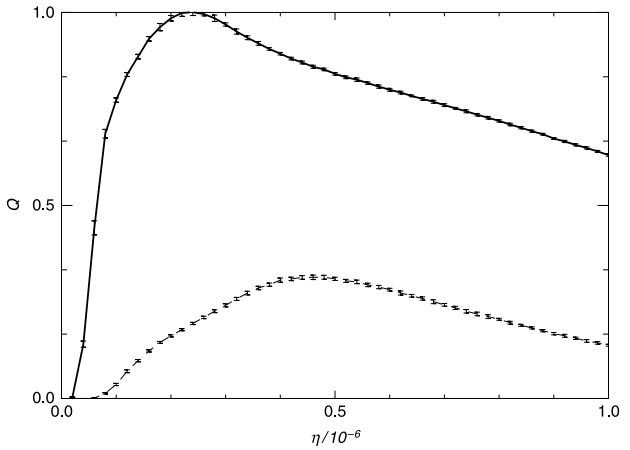

Fig. 8. Q-factor for network I (solid line) and network II (dashed line) as a function of noise intensity, averaged over 20 realizations and 42 signal periods, for $E = 2 \times 10^{-3}$.

stable and the resulting structure is shown as a stripe pattern for the activity record, which eventually degrades for larger levels of noise.

Even in this case noise does play a constructive role, and there is a particular level of noise where network I reaches the highest synchronization. We illustrate this point in Fig. 8, where the corresponding Q-factor presents a maximum at $\eta \approx 2.5 \times 10^{-7}$. At variance with the previous case, here the Q-factors of both networks do not exhibit their maxima at the same noise level. In fact, there is a decrease of Q in network II due to noise degradation, and there is also a shift in the position of its maximum towards higher noise intensity ($\eta \approx 4.5 \times 10^{-7}$).

4. Theoretical description of the dynamics through the NEP

The nonequilibrium potential (NEP) Φ for Langevin-type equations has been defined [28] through the zero-noise limit of the logarithm of the stationary probability density function

$$\lim_{\eta \to 0} P^{\text{stat}}(\mathbf{W}, \eta) = Z(\mathbf{W}) \exp\left[-\frac{\Phi(\mathbf{W})}{\eta} + \mathcal{O}(\eta)\right], \tag{8}$$

where $\mathbf{W}$ are the variables of the problem. Another way to introduce the NEP which remains valid even outside the small noise limit was proposed by Ao [43,44]. The NEP is a Lyapunov functional of the deterministic dynamics and provides information on the properties of attractors. In particular, it determines the height of the barriers separating attraction basins, which in turn define the transition rates among the different attractors.

The NEP for a general network of linearly coupled FitzHugh–Nagumo cells has been derived in Ref. [24]. Since the two networks defined in our model determine in turn a single network with a particular coupling structure, we can apply the results of Ref. [24] to the present case, obtaining

$$\Phi = \sum_{i=1}^{N} \left[\Phi_s(u_i, v_i) + \Phi_s(p_i, q_i) - \frac{2}{\lambda_1} S(t) u_i + \frac{2D}{\lambda_1}(u_i u_{i+1} + p_i p_{i+1}) + \frac{E}{\lambda_1}(u_i - p_i)^2 \right], \tag{9}$$

$$Z = \text{constant}, \tag{10}$$

with Φ_s being the NEP for a single cell without signal, given by

$$\Phi_s(u, v) = \frac{\epsilon}{\lambda_2}(v^2 - 2\beta\, uv - 2Cv) + \frac{2\lambda\epsilon}{\lambda_1\lambda_2}(\beta\, u^2 + 2Cu) - \frac{2}{\lambda_1}\left[\frac{b}{2}u^2 - \frac{b}{4}u^4\right],$$

where $\lambda_1 = r_1^2 + r_2^2$, $\lambda_2 = r_3^2 + r_4^2$ and $\lambda = r_1 r_3 + r_2 r_4$. Integrability conditions – arising from the NEP's derivation – constrain the parameters to obey

$$\beta\lambda_1 + \lambda_2/\epsilon = 2\lambda. \tag{11}$$

The third term in Eq. (9) is the explicit contribution of the signal (applied only to network I), the fourth one takes into account the antiphase-coupling inside each network and the last one, the electrical coupling between both rings.

A theoretical study of the dynamics can be done by exploiting the properties of the NEP during time-evolution. To this end we consider a simplified model, where each network is represented by a two-neuron system: a minimal description of an idealized case where all the even nodes on one hand, and all the odd nodes on the other, have the same stochastic phase–space trajectory. For this four-neuron model, the NEP in Eq. (9) takes the form:

$$\begin{aligned}\Phi(u_1, v_1, \ldots, p_2, q_2) = {} & \Phi_s(u_1, v_1) + \Phi_s(u_2, v_2) + \Phi_s(p_1, q_1) + \Phi_s(p_2, q_2) - \frac{2}{\lambda_1} S(u_1 + u_2) \\ & + \frac{4D}{\lambda_1}(u_1 u_2 + p_1 p_2) + \frac{E}{\lambda_1}[(u_1 - p_1)^2 + (u_2 - p_2)^2].\end{aligned} \tag{12}$$

The critical points (minima and saddles) of the NEP are the fixed points of the dynamics, and can be alternatively determined by the intersection of the nullclines. Although Eqs. (1)–(4) are not gradient, the non variational contribution to the dynamics also vanishes at the fixed points due to the particular structure of the probability current [24].

As far as we are interested only in barrier heights $\Delta\Phi$ – given by the difference in NEP between saddle points and minima – we project out the NEP along the slow manifolds, that capture all the system's fixed points. Thus we concentrate on $\Phi(u_1, u_2, p_1, p_2) = \Phi(u_1, \beta u_1 + C, u_2, \beta u_2 + C, p_1, \beta p_1 + C, p_2, \beta p_2 + C)$ and proceed to characterize their minima and saddles.

By U, E and S we represent the uniform, excited and "saddle" states in each network of the reduced model, respectively. In U both neurons remain inhibited (typically $u_1 \approx u_2 \approx -1$ for network I), which corresponds to the rest state in the real network. E represents one neuron excited and the other one inhibited (for example $u_1 \approx -u_2 \approx 1$ in network I), which corresponds to an APS in the real network. Finally S is an intermediate state (for example $u_1 \approx -1$ and $u_2 \approx 0$ in network I), that corresponds to a transition between rest state and APS in the network.

We introduce a two-letter code to label the fixed points of the reduced model, where the first letter corresponds to network I while the second one corresponds to network II. Accordingly, UU represents both networks in the uniform state, while EE denotes both networks in excited states. A subindex two in the code means that the inhibited neurons in each network are not electrically connected between them. Accordingly, for example, the state where $u_1 \approx -p_1 \approx p_2 \approx -1$ and $u_2 \approx 0$ is labeled SE_2. It is worth noting that if at least one letter in the code is S, the whole state corresponds to a saddle point in the NEP. This is why we label with S such single-network intermediate state. All states and saddles of the reduced model except UU are degenerate – same stability and NEP value – under simultaneous permutations of u_1 by u_2 and p_1 by p_2. Note that interchanging simultaneously u_1 by p_1 and u_2 by p_2 generally results in a different NEP value, because u_i and p_i are not equivalent except for $S = 0$ (the signal breaks the symmetry between networks).

As we will see, the dynamics can be mainly interpreted as a succession of noise-activated transitions between metastable attractors, whose relative stability is ruled by the NEP. The process to escape from a given minimum through a barrier is an activation process, where the energy for the jump comes from the noise. To estimate the noise intensity to escape, we compare the NEP fluctuations $\sigma_\Phi^2 = \langle\Phi^2\rangle - \langle\Phi\rangle^2$ with the barrier height $\Delta\Phi$ that confines the metastable attractor, resulting[4]

$$\eta \approx \frac{\Delta\Phi}{\sqrt{2}}. \tag{13}$$

[4] Expanding Φ up to second order around its minimum, the probability density function given by Eq. (8) is a Gaussian, yielding the approximate expression $\sigma_\Phi^2 = n\eta^2/2$, where n is the number of neurons (four in the reduced model).

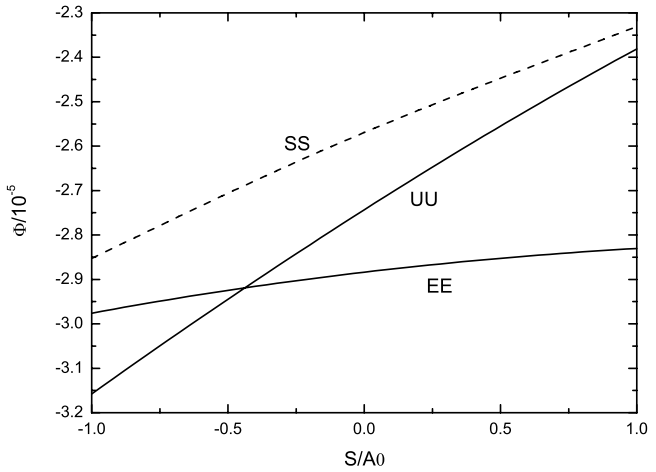

Fig. 9. NEP values in the minima (solid lines) and saddles (dashed line) of the four-neuron model, for $E = 2 \times 10^{-2}$.

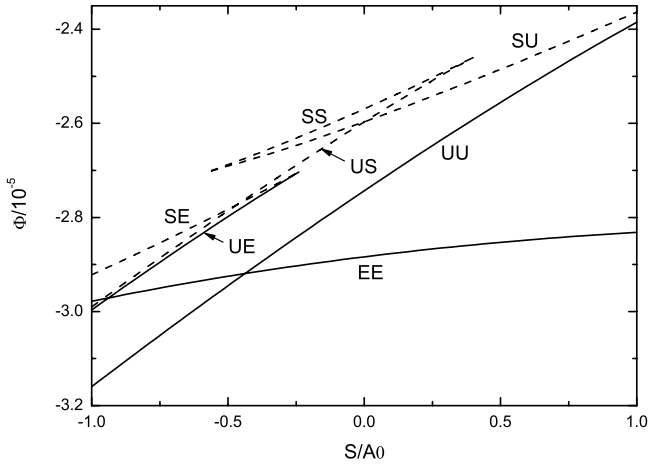

Fig. 10. NEP values in the minima (solid lines) and saddles (dashed lines) of the four-neuron model, for $E = 8 \times 10^{-3}$.

To elucidate the dynamics, we proceed to consider the behavior of the NEP in terms of the signal for the attractors and repellers involved in each route to synchronization. In all cases, it is assumed that the system starts from the UU state (as in the simulations).

For high enough electric coupling ($E > 10^{-2}$), the reduced model has a UU state, two EE states and two saddles SS whose NEP defines the barrier in the transition UU $\rightarrow$ SS $\rightarrow$ EE. In Fig. 9 we represent the NEP in minima and saddles as a function of the value of the adiabatic signal for $E = 2 \times 10^{-2}$. For small η, the barrier to escape from the UU state cannot be reached, and the system (both networks) can only perform small oscillations around the rest state. According to Eq. (13), for a noise intensity $\eta \approx 3.5 \times 10^{-7}$ the barrier can be overcome at $S = A_0$, and consequently the EE state – with a lower potential – is reached. But once in the EE state, the new barrier to escape is higher and then both networks remain simultaneously activated, as we show in Fig. 1(b). The noise level must be raised to $\eta \approx 8.7 \times 10^{-7}$ to overcome the new barrier at $S = -A_0$ and return to the UU state. This noise level is the NEP's prediction for the complete synchronization, that is in good agreement with the maximum of the Q-factor (see Fig. 3).

For weaker coupling ($E < 10^{-2}$) a new metastable state UE appears for same values of the external signal. Simultaneously, a more intricate structure of saddles SE, SS, SU and US appear to complete the potential landscape, as can be seen in Fig. 10 for $E = 8 \times 10^{-3}$. As usual, only subthreshold oscillations (in UU state) are present in both rings for small η. Increasing the noise level to $\eta \approx 1.5 \times 10^{-7}$, the EE state is reached through the SU state at $S = A_0$. The noise level must be raised to $\eta \approx 4 \times 10^{-7}$ in order to return to UU and close the cycle of synchronization. Thus, the dynamics with this NEP structure turns out to be basically similar to the cases with higher E discussed before. Nevertheless, in the escape from EE through SE (at $S = -A_0$) the metastable state UE is achieved but their confining barrier – represented by US (approximately 6×10^{-8}) – is immediately overcome to reach UU. Paradoxically in the UE, the externally forced network remains at rest while the second one is driven to the APS. UE states, although not macroscopically occupied, can be generated by appropriate initial conditions: numerical simulations (not shown) confirm their existence and the noise level for decay.

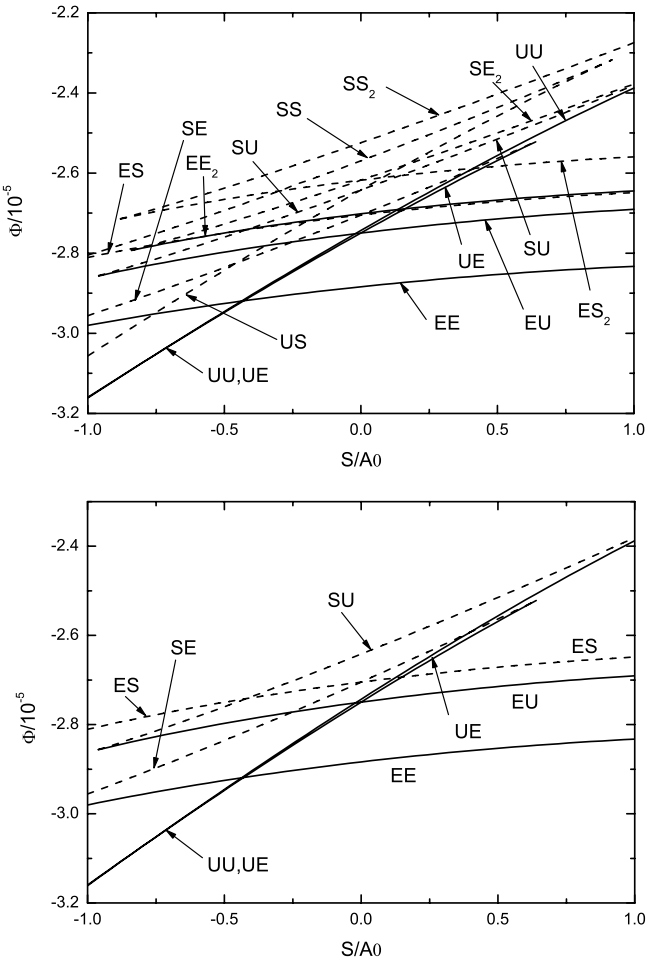

Fig. 11. NEP values in the minima (solid lines) and saddles (dashed lines) of the four-neuron model, for $E = 2 \times 10^{-3}$. In the upper panel, all the 9 (UU plus four two-folded) minima and 16 (8 two-folded) saddles are identified. The lower panel is a simplified graph with the most relevant curves, for a clearer view. Curves corresponding to UE (close to UU, but different) collapse with SE at $S/A_0 = 0.64$, where both disappear. Similarly, EU collapses with SU and both disappear at $S/A_0 = -0.96$.

By decreasing the electrical coupling below 6×10^{-3} we find a richer dynamics, where the networks are not restricted to stay in the same state (see Figs. 6 and 7). This behavior is also captured by the reduced model, which in this case exhibits a complex structure of fixed points, as we illustrate in Fig. 11 for $E = 2 \times 10^{-3}$. To elucidate the observed dynamics in this regime, we show the NEP vs. signal behavior of the relevant states in the lower panel of Fig. 11. Again, subthreshold oscillations take place in the UU state, and the system remains in this regime for small noise. A noise level $\eta \approx 4.7 \times 10^{-8}$ allows the system to climb the barrier given by SU (at $S = A_0$) to reach the EU state. This state disappears by collapsing with the SU saddle before S reaches $-A_0$, and the system returns deterministically to the UU state, completing the cycle. This is the dynamics shown in Fig. 6(c) and (d), where network I is synchronized with the signal while network II remains in the U state. In this case, the noise level for synchronization of network I is determined by the activation barrier in the transition UU $\rightarrow$ SU $\rightarrow$ EU, that keeps network II at rest.

In order to activate network II, we must increase the noise level to $\eta \approx 2.9 \times 10^{-7}$; then, the system can escape from EU (before it collapses) through the ES barrier, to reach the EE state (which has a lower NEP). The barrier to escape from EE – determined by the SE saddle – is overcome at $S = -A_0$ (where it is smaller than the EU–ES barrier) to reach the UE state. This state eventually disappears before S reaches A_0, and the system returns deterministically to EE. Summarizing, the system passes adiabatically with the signal from UE to EE; in other words, while network I is synchronized with the signal, network II remains in the APS, as we numerically observe in Fig. 7(a) and (b).

For a synchronization of both networks with the external signal it is necessary to alternate between EE and UU states. The barrier to escape from EE – determined by the US saddle – is the higher barrier in the chain of transitions EE $\rightarrow$ SE $\rightarrow$ UE $\rightarrow$ US $\rightarrow$ UU and requires $\eta \approx 7.3 \times 10^{-7}$ (at $S = -A_0$). This is in consequence the theoretical prediction for the maximum Q-factor in network II (which results higher than that obtained from simulations, shown in Fig. 8). However, as we have seen before, this noise level is sufficient to overcome the lower barrier to UE and let the system pass randomly to UU or UE (but

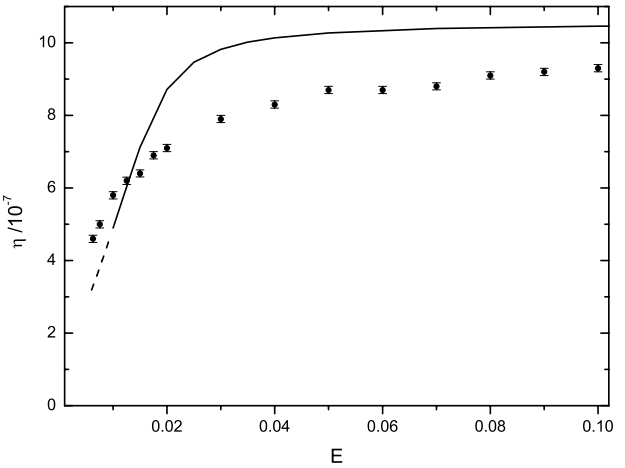

Fig. 12. Four-neuron model prediction of the noise level for best synchronization: the solid line corresponds to the attractor-barrier structure in Fig. 9, the dashed line to the one in Fig. 10, and the points to maxima of the Q-factor computed from simulations (averaged over 20 realizations).

more often to UE, due to its lower barrier height). Besides, the high noise level degrades the synchrony of network I with the signal (see the height difference of both maxima in Fig. 8). As a consequence (at variance with the previous cases, where the coupling strength between networks E is higher) a clear synchronic regime of both networks with the signal cannot be reached for these parameters.

We summarize the results for full synchronization of both networks with the external signal in Fig. 12, where we have plotted the maximum Q-factor obtained from simulations for some values of electrical coupling, together with the prediction of the four-neuron model. From the graph we can see that the theoretical curve saturates for $E \to \infty$. By noting that in this limit $u_i = p_i$, Eq. (12) simplifies to

$$\Phi = 2[\Phi_s(u_1, v_1) + \Phi_s(u_2, v_2)] - \frac{2}{\lambda_1} S(u_1 + u_2) + \frac{8D}{\lambda_1} u_1 u_2, \tag{14}$$

that has a similar attractor structure to that represented in Fig. 9, resulting $\eta = 1.05 \times 10^{-6}$ for the saturation value. Even when the four-neuron model estimation of η for best synchronization is crude, such a reduced model captures the trend and the order of magnitude of optimal noise synchronization.

5. Conclusions

We have presented analytical and numerical results for the stochastic dynamics of two electrically coupled networks of excitable FitzHugh–Nagumo neurons, each of them phase-repulsively linked to form a ring.

With the aim of characterizing the capability of electrical couplings to "transfer" a noise-sustained synchronized state from one network to the other, only one of the rings has been externally and adiabatically forced by a subthreshold harmonic signal. On the other hand, the whole system was submitted to additive and independent Gaussian white noises with the same intensity η.

Numerical integration for appropriate parameter values shows that local additive noise sustains extended antiphase-state (APS) – where the cells alternate their activation state – in both rings, which moreover synchronize with the external subthreshold signal. Coherent behavior is then observed, where both networks exhibit essentially the same synchronized activity. Moreover, the Q-factors exhibit maxima as functions of η. The role of the noise is thus twofold: on one hand, it is an essential ingredient for the phenomenon to occur; on the other, there is an optimal noise intensity for maximal coherence.

The route to synchronization was also considered. For small electrical coupling, we have shown the existence of regimes where only partial activation takes place: one network activates (and even synchronizes in a noise-sustained fashion), while the other ring remains at rest.

The numerical results can be better interpreted and quantitatively accounted for with reasonable accuracy by considering the nonequilibrium potential (NEP) of a four-cell reduced model. Basically, it is the (adiabatic) stationary probability density – in the limit of small noise – whose structure of minima (attractors) was completely analyzed and the potential barriers (saddle points) of the allowed transition were all identified.

The four-cell approach does not take into account the formation of defects in the networks, which break the background activation alternance of extended APS. Nevertheless, the theoretical results help elucidate the route to synchronization between networks, identify the relative stability of the relevant states and estimate the order of magnitude of the optimal noise intensity for activation and synchronization.

By analyzing the dependence of the potential barriers on the external signal, we have shown that the observed dynamics can be explained in terms of noise-sustained transitions between attractors and (eventually) deterministic collapse. The

theoretical analysis also allowed to identify a curious regime where the externally forced network remains at rest, while the second one results activated. Although in the context of the present work this state does not play any central role, it could be relevant in the context of processing and transmission of information by electro-chemical signaling. As it occurs for related phenomena (e.g. coherence resonance in coupled FitzHugh–Nagumo systems [35]), our results are expected to depend on both temporal and spatial noise correlations. The NEP approach would be useful even in those cases, since dynamics driven by space-correlated or colored (OrnsteinUhlenbeck) noises can in principle be described in terms of a suitable NEP [45].

Acknowledgments

We acknowledge financial support from CONICET (project PIP 220100100315) and Universidad Nacional de Mar del Plata (project 15/E639), of Argentina. We also thank R. Deza for his critical reading of the manuscript.

References

[1] K.V. Baev, Biological Neural Networks: Hierarchical Concept of Brain Function, Birkhäuser, Boston, 1998.
[2] M.A. Arbib (Ed.), The Handbook of Brain Theory and Neural Networks, second ed., MIT Press, Cambridge, 2003.
[3] P.J. Uhlhaas, W. Singer, Neuron 52 (2006) 155.
[4] L.M. Ward, Contemp. Phys. 52 (2009) 563.
[5] J.M. Casado, Phys. Lett. A 310 (2003) 400.
[6] Z.F. Mainen, T.J. Sejnowski, Science 268 (1995) 1503.
[7] J. Pang, C. Monterola, J. Bantang, Physica A 393 (2014) 638.
[8] Q. Wang, et al., Physica A 387 (2008) 4404.
[9] H.D.I. Abarbanel, M.I. Ravinovich, A. Selverston, M.V. Bazhenov, R. Huerta, M.M. Sushchik, L.L. Rubchinskiĭ, Phys. Usp. 39 (1996) 337.
[10] J.H. Byrne, W.O. Berry (Eds.), Neural Models of Plasticity: Experimental and Theoretical Approaches, Academic Press, San Diego, 1989.
[11] C.M. Gray, J. Comput. Neurosci. 1 (1994) 11.
[12] R. Eckhorn, Time and the Brain, Harwood, Academic Publishers, 2000, pp. 169–201.
[13] F.H. Lopes da Silva, J.P.M. Pijn, J.A. Gorter, E. van Vliet, E.W. Daalman, W. Blanes, Chaos in Brain, World Scientific, Singapore, 2000.
[14] F.J. Varela, J.-P. Lachaux, E. Rodriguez, J. Martinerie, Nat. Rev. Neurosci. 2 (2001) 229.
[15] L. García Dominguez, R. Wennberg, W. Gaetz, D. Cheyne, O.C. Snead, J.L. Perez Velazquez, J. Neurosci. 25 (2005) 8077.
[16] D. Guo, Q. Wang, M. Perc, Phys. Rev. E 85 (2012) 061905.
[17] M.S. Baptista, F.M. Moukam Kakmeni, C. Grebogi, Phys. Rev. E 82 (2010) 036203.
[18] M.R. Deans, J.R. Gibson, C. Sellitto, B.W. Connors, D.L. Paul, Neuron 31 (2001) 477.
[19] G. de Vries, A. Sherman, in: S. Coombes, P.C. Bressloff (Eds.), The Genesis of Rhythm in the Nervous System, World Scientific, Singapore, 2005.
[20] S. Dhein, J.S. Borer (Eds.), Cardiovascular Gap Junctions, in: Advances in Cardiology, S. Karger, Basel, 2006.
[21] M. Bennett, J. Contreras, F. Bukauskas, J. Sáez, Trends Neurosci. 26 (2003) 610.
[22] G.G. Izús, R.R. Deza, A.D. Sánchez, AIP Conf. Proc. 887 (2007) 89.
[23] G.G. Izús, A.D. Sánchez, R.R. Deza, Physica A 388 (2009) 967.
[24] A.D. Sánchez, G. Izús, Physica A 389 (2010) 1931.
[25] M. dell'Erba, G. Cascallares, A.D. Sánchez, G. Izús, Eur. Phys. J. B 87 (2014) 82.
[26] G. Izús, R.R. Deza, H.S. Wio, Phys. Rev. E 58 (1998) 93.
[27] G.G. Izús, R.R. Deza, H.S. Wio, Comput. Phys. Comm. 121–122 (1999) 406.
[28] R. Graham, in: E. Tirapegui, D. Villarroel (Eds.), Instabilities and Nonequilibrium Structures, D. Reidel, Dordrecht, 1987, pp. 271–290.
[29] F. Sagués, J.M. Sancho, J. García-Ojalvo, Rev. Modern Phys. 79 (2007) 829.
[30] H.S. Wio, R.R. Deza, Eur. Phys. J. Spec. Top. 146 (2007) 111.
[31] H.S. Wio, S. Bouzat, B. von Haeften, Physica A 306 (2002) 140.
[32] J.A. Acebrón, A.R. Bulsara, W.J. Rappel, Phys. Rev. E 69 (2004) 026202.
[33] J. García-Ojalvo, J.M. Sancho, Noise in Spatially Extended Systems, Springer, New York, 1999.
[34] R. Toral, C.J. Tessone, J. Viana Lopez, Eur. Phys. J. Spec. Top. 143 (2007) 59.
[35] A.S. Pikovsky, J. Kurths, Phys. Rev. Lett. 78 (1997) 775.
[36] L. Gammaitoni, P. Hänggi, P. Jung, F. Marchesoni, Rev. Modern Phys. 70 (1998) 223.
[37] K. Wiesenfeld, F.J. Jaramillo, Chaos 8 (1998) 539.
[38] T. Wellens, V. Shatokhin, A. Buchleitner, Rep. Progr. Phys. 67 (2004) 45.
[39] H.S. Wio, Phys. Rev. E 54 (1996) R3075.
[40] C. Zhou, J. Kurths, B. Hu, Phys. Rev. E 67 (2003) 030101(R).
[41] G.V. Osipov, J. Kurths, C. Zhou, Synchronization in Oscillatory Networks, Springer, Berlin, 2007.
[42] N.B. Janson, A. Galanov, E. Schöll, Phys. Rev. Lett. 93 (2004) 010601.
[43] P. Ao, J. Phys. A: Math. Gen. 37 (2004) L25.
[44] L. Yin, P. Ao, J. Phys. A: Math. Gen. 39 (2006) 8593.
[45] A. Schenzle, T. Tél, Phys. Rev. A 32 (1985) 596.